JMATPRO	Journal of Advanced Materials and Processing 10 (4): 25-35, Autumn 2022 http://jmatpro.iaun.iau.ir 20.1001.1.2322388.2022.10.4.3.2

Research Paper

Synthesis and Characterization of Linear/Nonlinear Optical Properties of GO, RGO, RGO-ZNO, and RGO-ZNO-Fe_2O_4

Mohsen Ebrahimi Naghani[1], Mina Neghabi[1*], Mehdi Zadsar[1], Hossein Abbastabar Ahangar[2]

1. Department of Physics, Najafabad Branch, Islamic Azad University, Najafabad, Iran.

2. Department of Chemistry, Najafabad Branch, Islamic Azad University, Najafabad, Iran.

ARTICLE INFO

Article history:

Received 08 April 2022
Accepted 6 July 2022
Available online 1 September 2022

Keywords:
Linear and nonlinear optical properties
Reduced graphene oxide
Nanocomposite
Z-Scan.

ABSTRACT

In this paper, we aimed to investigate the linear and nonlinear optical properties of reduced graphene oxide-based metal oxide nanocomposite in comparison with reduced graphene oxide (RGO) and the effect of the process of reducing the oxygen groups of graphene oxide on the change of the nonlinear absorption coefficient of the reduced graphene oxide- zinc oxide (RGO-ZnO) and reduced graphene oxide-zinc oxide-iron oxide (RGO-ZnO-Fe_2O_4) sample. For this purpose, RGO, RGO-ZnO, and RGO–ZnO-Fe_2O_4 were synthesized using Hummers and hydrothermal methods, respectively, and then were analyzed using Fourier transform infrared (FT-IR), Ultraviolet-visible absorption (UV-Vis), energy dispersive X-ray spectroscopy (EDX), and X-ray diffraction (XRD) were characterized. The XRD and FTIR analysis successfully synthesized RGO-ZnO and RGO-ZnO-Fe_2O_4 nanocomposites. Also, FT-IR spectroscopy indicated that absorption bands at 3340 cm^{-1}, 1630 cm^{-1}, 1730 $cm^{-1,}$ and 480 cm^{-1} are related to O-H, C=C, C=O, and Zn-O stretching vibrations, subsequently. The direct energy gap of GO, RGO, RGO-ZnO, and RGO-ZnO-Fe_2O_4 from UV-Vis spectra was reported to be 3.36, 3.18, 3.25, and 2.7eV, respectively. In addition, the third-order nonlinear optical properties (the nonlinear absorption coefficient) of all samples were investigated using the Z-scan technique with Nd: YAG laser (532 nm, 70 mW), and it was observed that the third-order nonlinear optical properties were increased from 8.3×10^{-4}cm/W for RGO to 5.6×10^{-3} cm/W for RGO-ZnO-Fe_2O_4.

Citation: Ebrahimi Naghani, M.; Neghabi, M.; Zadsar, M.; Abbastabar Ahangar, H. (2022). Synthesis and Characterization of Linear/Nonlinear Optical Properties of GO, RGO, RGO-ZNO, and RGO-ZNO-Fe2O4, Journal of Advanced Materials and Processing, 10 (4), 25-35. Dor: 20.1001.1.2322388.2022.10.4.3.2

* **Corresponding Author:**
E-Mail: Neghabi@iaun.ac.ir

1. Introduction

Graphene is one of the thinnest and flattest materials that could ever be in the universe. As it has a unique two-dimensional structure, much research has been done on its excellent properties, such as high mechanical flexibility, electrical-thermal conductivity, and chemical stability [1-11]. Because of these characteristics, graphene has various applications in supercapacitors [12, 13], photovoltaics [14-16], fuel cells [17, 18], sensors [19, 20], and nanofluids [21, 22]. The two-dimensional crystal structure of Graphene can make it more popular to load diverse nanocomposites [23]. For example, composites of graphene and metal oxides have shown higher performance for energy storage [24-27] and electrochemical detection [28-31] compared to pure graphene. Research on reduced graphene has demonstrated that graphene composites exhibit significant nonlinear optical (NLO) responses [32]. Recently, combinations of graphene and metal oxides have attracted considerable attention because of their broad utilization in catalysis, water purification, hydrogen production, lithium-ion batteries, and transparent electronics [33-38]. For example, zinc oxide (ZnO) is an inorganic metal oxide with a wide band gap of 3.37 eV [39, 40] and a large exciton binding energy at room temperature (60 meV) has many potential applications such as light-emitting diodes [41], solar cells [42-45], sensors [46-48], photodetectors [49], and nanogenerators [1, 5]. The main criterion in the nonlinear optical process is to find a nonlinear optical material with high-intensity application based on a nonlinear absorption coefficient (β). For applications like sensors, bio-medical, and optoelectronic devices, ZNO-Fe_2O_4 is widely used due to its specific optical applications [40].

As a result, according to the individual properties of graphene, ZnO, and Fe_2O_4, combining graphene with ZnO and Fe_2O_4 nanoparticles can enhance performances [1]. One of the possible methods to improve the poor solubility of graphene is the oxidation of graphene and modification of GO with some soluble materials. Since GO has large quantities of oxygen-containing groups such as carboxyl, carbonyl, and hydroxyl/epoxy, it can provide various decoration ways with organic and inorganic materials by covalent/non-covalent functionalization [50].

Numerous techniques have been documented for synthesizing graphene oxide (GO) and reduced graphene oxide (RGO). Common methods for GO synthesis include chemical vapor deposition, mechanical exfoliation, electron-beam evaporation, Staudenmaier [51], Hofmann [52], Jaleh [53], Marcano [54], and Hummers' method. Among them, the Hummers' method is widely used for the production of GO today [55]. Reduction of GO can be accomplished through chemical, thermal, optical, and hydrothermal methods. Consequently, there is a need for cost-effective and scalable production of RGO. Among the methods employed, the modified Hummer method is widely accepted for its high efficiency. Conversely, alternative approaches for producing GO and RGO involve multiple steps, chemicals, and solvents, resulting in time-consuming procedures. In addition, while different methods have been used to synthesize metal oxide-graphene composite materials, the hydrothermal approach stands out due to its high growth rate, cost-effectiveness, and simplicity [56].

As assumed, a combination of graphite with metal oxides can enhance optoelectronic properties. For this purpose, the linear and nonlinear optical properties of the RGO-ZnO-Fe_2O_4 hybrid were studied in this work. First, a modified Hummers' method synthesized GO directly from the graphite. Then, the nanocomposite of RGO-ZnO-Fe_2O_4 was fabricated using the hydrothermal method. The structural properties of samples were investigated using powder X-ray diffraction (XRD), Energy-dispersive x-ray (EDX), and Fourier-transform infrared (FT-IR) spectra. The optical properties of samples were analyzed by UV-visible spectroscopy and Z-scan analysis. Finally, we studied the nonlinear optical properties of GO, RGO, RGO-ZnO, and RGO-ZnO-Fe_2O_4 using Z-scan analysis. The results show that the nonlinear optical properties of the RGO-ZnO-Fe_2O_4 composite are enhanced compared to GO and RGO. Therefore, RGO-ZnO-Fe_2O_4 nanocomposite can be a good candidate for optical communication and storage [32].

The structural defects in graphene, such as vacancies and edges, give rise to characteristic Raman spectroscopic peaks known as the G-band and the D-band. The intensity ratio of the D-band (associated with defects) to the G-band (related to the crystalline structure) is represented by the ID/IG ratio. The ID/IG ratio indicates the degree of disorder and the presence of defects in graphene-based materials. When graphene oxide (GO) is reduced to reduced graphene oxide (RGO), the ID/IG ratio can increase compared to GO. This is due to the restoration of sp^2 carbon bonds and a reduction in the average sizes of sp^2 domains upon reduction. The higher intensity of the D-band suggests the presence of more isolated graphene domains in RGO compared to GO. In the case of the RGO-ZnO sample, the increased ID/IG ratio (compared to GO layers) implies the chemical reduction of GO. Overall, a high ID/IG ratio indicates a significant level of disorder, likely indicating a beneficial integration of RGO with ZnO [57].

In Hummers' method, single-layer graphene cannot directly be obtained, and graphene oxide straightly is gained. Since there is a problem that many

characteristics of single-layer graphene are lost in graphene oxide, it is aimed to prove that by reducing oxygen groups, the nonlinear optical properties in RGO increased compared to GO. In addition, the combination of RGO and metal oxides can improve non-linear optical properties. This study developed a novel approach for comparing the properties of GO, RGO, RGO-ZnO, and RGO-ZNO-Fe_2O_4. Moreover, the non-linear optical properties of graphene and reduced graphene oxide were investigated simultaneously. After combining metal oxides, it was shown that many unique properties of graphene could be returned by reducing oxygen groups. Although it has been pointed out in previous works that combining graphene and metal oxides can improve the optical properties, there is no comparison between linear and non-linear optical properties of graphene oxide and graphene oxide nanocomposites reduced with metal oxides.

2. Experimental

First, pure graphite was used, and graphene oxide, using Hummers' method, was obtained. As the properties of single-layer graphene are wanted, In the next step, we synthesized RGO to return to some of the properties of single-layer graphene. In the final step, Fe and Zn metal oxides were also synthesized with RGO by Hydrothermal method. As the third-order nonlinear optical characteristics of GO, RGO, RGO-ZnO, and RGO-ZnO-Fe_2O_4 samples can be studied using the Z-scan technique, the second harmonic of a Q-switched Nd: YAG laser (532 nm, 4 ns) was used as the laser source (Fig. 1).

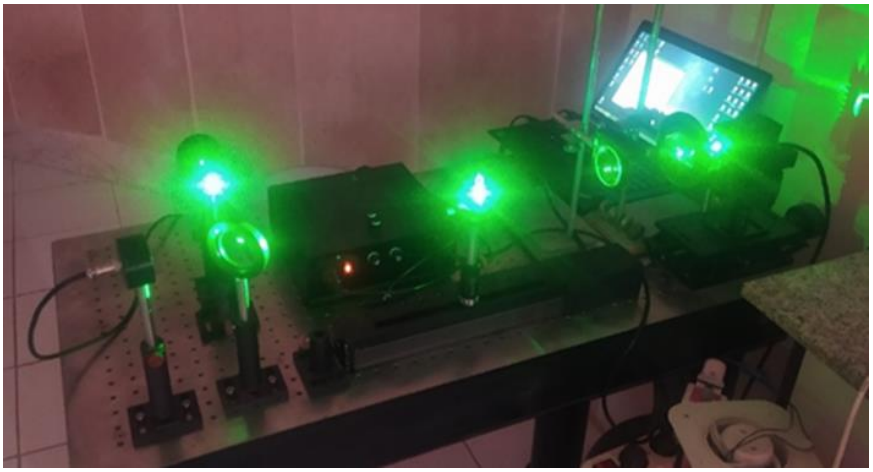

Fig. 1. Z-scan analysis laboratory setup

2.1. Materials

Spectroscopically pure (SP) graphite, sulfuric acid (H_2SO_4), hydrogen peroxide (H_2O_2), Potassium hydroxide (KOH), hydrazine hydrate (N_2H_4), Zinc acetate dehydrate Zn $(CH_3COO)\cdot 7H_2O$ potassium permanganate ($KMnO_4$), Ferric Chloride, ($FeCl_3$) and Sodium hydroxide (NaOH) were purchased from Merck chemical company and used without any purification.

2.2. Synthesis of Graphene Oxide (GO)

First, 0.2 g graphite was mixed with concentrated H_2SO_4 (50 ml) and stirred for 12 h. Then, the mixture was cooled in an ice bath under vigorous stirring, and at the same time, $KMnO_4$ (2.5 g) was added slowly to the suspension and stirred for 2.5 h. The solution was diluted with distilled water (50 ml), and the stirring was continued for one h. The mixture was further allowed to cool down to room temperature and finally treated with 50 ml distilled water, followed by 100ml H_2O_2 30%. Then, it was purified by centrifuging and washing with excess water until the pH reached 7 to obtain GO [55].

2.3. Synthesis of Reduced Graphene Oxide (RGO)

Graphite oxide was dispersed in deionized water by sonication for two h. Then, 0.6 g KOH (purity 99.5%) and 4 mL hydrazine hydrate (concentration 80%) were added to the suspension, and the temperature increased up to 100 °C and re-fluxed for 24 h. Ultimately, the obtained RGO was washed and dried [51].

2.4. Preparation of RGO-ZnO Nanocomposite

To prepare GO-ZnO nanocomposite with the mass ratio of 10% GO, 2.7 g of Zn $(CH_3COO).7H_2O$ was added to 30 mL deionized water, and then 0.05 g GO was added under low-speed stirring. After that, NaOH 3M was added to the above solution slowly until pH reached 12, and the resulting mixture is ultrasonication for 30 minutes. The final mix was transferred to a Teflon-lined autoclave for hydrothermal synthesis at 160 ℃ in an oven for 20 h. The precipitate (GO-ZnO) was washed three times with deionized water and acetone and dried at 80 ℃.

To obtain RGO-ZnO, the mentioned stages were repeated with 0.05 g of RGO.

2.5. Synthesis of RGO-Zn-Fe_2O_4-10% Nanocomposite

2.1 gr of $FeCl_3$ and 2.2 gr of Zn $(CH_3COO).7H_2O$ were added to 30 ml of deionized water. Then 0.3 gr of GO was separately added to 30 ml deionized water. In the next step, both solutions were mixed slowly .After that, ammonia was added to the sample to increase the pH 11. In the next step, 5 cc. of hydrazine were added and stirred for 5 hours at 70 degrees.

There are extensive chemical and physical methods, such as top-down, bottom-up, sol-gel, and hydrothermal methods, for obtaining nanocomposites RGO and RGO-ZnO [58]. Also, some recent works have examined the method of creating ZnO-Fe by chemical spray pyrolysis [59]. In addition, RGO-$ZnFe_2O_4$ can be gained using the hydrothermal method [60]. The hydrothermal synthesis method can be a safe, low-cost, and good-quality crystal [58].

3. Results and discussion

3.1. Structural and elemental properties

Crystal structure quality and orientation of Graphite, GO, RGO, RGO-ZnO, and RGO-ZnO-Fe_2O_4 nanocomposite is provided in Fig. 2. According to the XRD pattern of GO, the sharp diffraction peak at 9° which is related to the basal spacing of GO (8.97 Å) and because of the intercalation of oxygen-containing groups, it is higher than Graphite (4 Å) [5]. In the graphite pattern, the sharp peak at 2θ=26.4 and wide peak at 24.42 in the RGO pattern are attributed to a carbon atom's (002) plane. The RGO-ZnO nanocomposite patterns show highly crystalline peaks at 2θ =31.9◦, 34.7°, 36.5°,47.7°, 56.8°, 63.0°, 66.6°, 67.9°, 69.2°, and 72.7°. They can be attributed to the high crystallinity of ZnO during the hydrothermal method that led to the disappearing characteristic peak of GO and RGO that are following single phase hexagonal structure with a space group of P6 3 mc (ICDD card number 01-079-0207). In addition, highly crystalline peaks were observed for RGO-ZnO-Fe_2O_4 nanocomposite at 2θ =29.8°, 35.4°, 43.2°, 53.6°, 56.9°, and 62.9° that are in agreement with spinel $ZnFe_2O_4$ phase matches well with the standard JCPDS card No. 22-1012 [61]. In addition, highly crystalline peaks were observed for RGO -ZnO-Fe_2O_4 nanocomposite at 2θ =29.8°, 35.4°, 43.2°, 53.6°, 56.9°, 62.9°. Notably, the XRD instrument is the Philips PW3040, with a wavelength of 1.54 Å and a step size of 0.05, and a copper lamp. Moreover, the results of The scanning electron microscope (SEM) and energy-dispersive X-ray (EDX) spectroscopy are provided in Fig. 3, which show the presence of Zn, C, S, Mn, K, Fe, and O atoms in our samples. Also, the elemental distribution and EDS spectrum indicate an apparent change in the oxygen group ratio from 34.08 (At%) in GO to 20.43 (At%) in RGO samples [5, 29].

The SEM, Philips XI30, is a powerful analytical instrument that employs a focused beam of electrons to interact with the sample, generating various signals that provide detailed information about the sample's properties. Its units of measurement are nm, and its measuring accuracy is 10 nm.

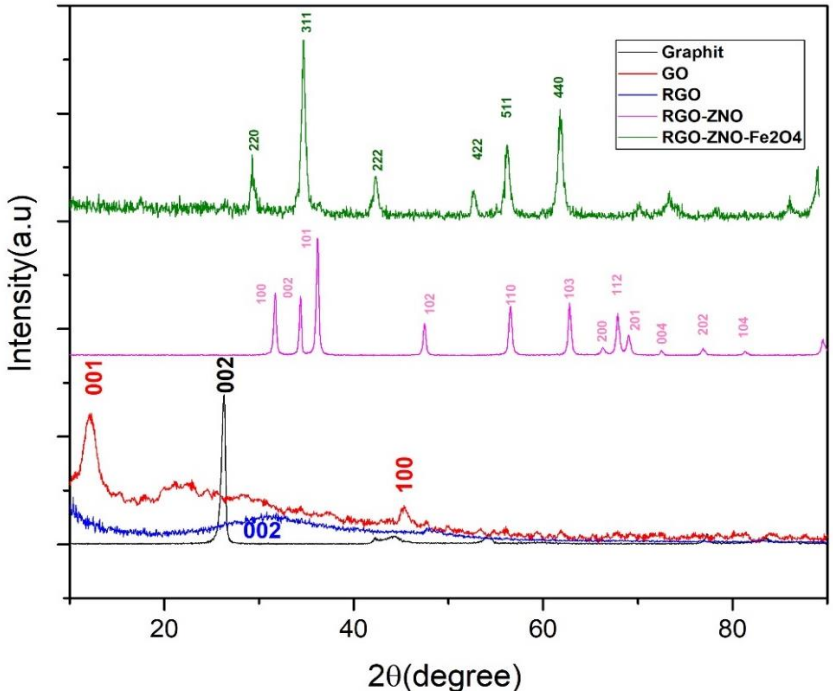

Fig. 2. XRD patterns of Graphite, GO, RGO, RGO-ZnO, and RGO-ZnO-Fe_2O_4 nanocomposites

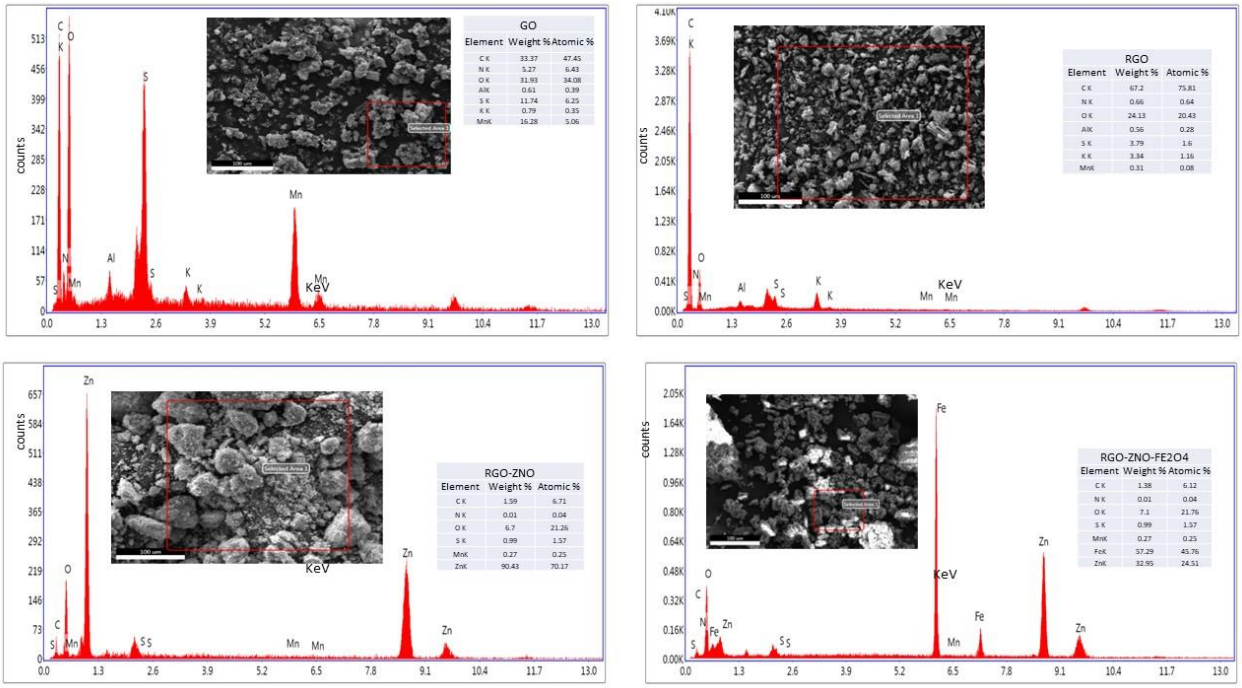

Fig. 3. Scanning electron microscopy with energy-dispersive X-ray spectroscopy (SEM-EDX) analysis for GO, RGO, RGO-ZnO, and RGO-ZnO-Fe_2O_4

3.2. FT-IR

The results of FTIR spectroscopy of GO, RGO, RGO-ZnO, and RGO-ZnO-Fe_2O_4 are shown in Fig. 4. The pattern of GO indicates an O-H group stretching vibration band at 3340 cm^{-1}. The sp^2 structure of C=C and carbonyl functional groups (C=O stretching) are observed at 1630 cm^{-1} and 1730cm^{-1}, respectively [23]. The absorption peak at 1220 cm^{-1} and 1044 cm^{-1} are attributed to the C-O stretching vibration band. It should be mentioned that the vibrations bands of O-H, C=O, and C-O have been significantly reduced, attenuated, and slightly shifted to a lower wavenumber which can result from deoxygenation in RGO. Finally, the absorption peaks at 568 cm^{-1} and 465 cm^{-1} in RGO-ZnO-Fe_2O_4 patterns can be attributed to ZnO and Fe_2O_4 stretching vibration.

It is to be noted that the FTIR spectrometer covers the mid-infrared (MIR) region, ranging from 2.5 to 25 micrometers (4000 to 400 cm^{-1}). In addition, the measuring accuracy of this instrument is 1.0.

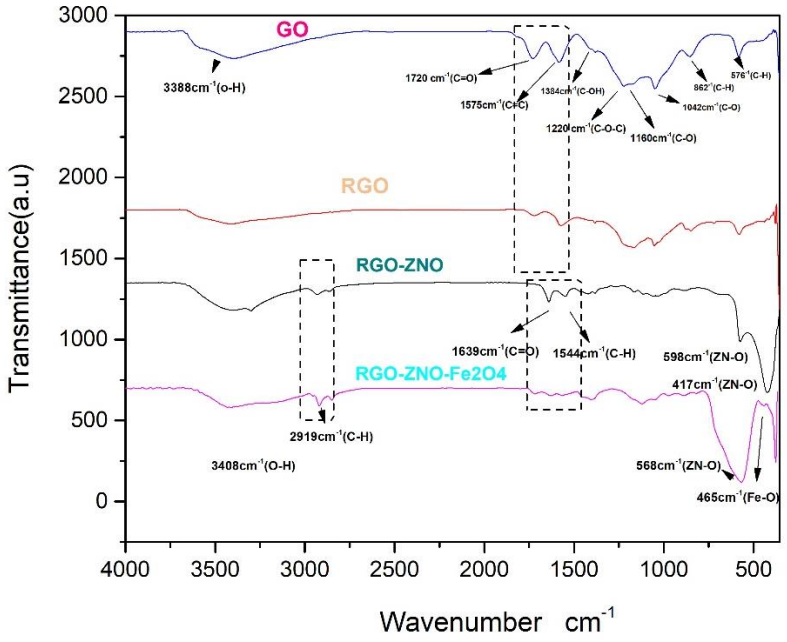

Fig. 4. FTIR spectra of GO, RGO, RGO-ZnO and RGO-ZnO-Fe_2O_4

3.3. UV-Vis absorption spectra

According to Fig. 5a, GO has an absorption peak at about 230 nm, which is probably caused by the $\pi \rightarrow \pi^*$ transition of C-C bonds, and also shows a smaller peak at about 300 nm, which corresponds to the $n \rightarrow \pi^*$ transition of the bond [62-65]. Whereas the peak of the $\pi \rightarrow \pi^*$ transition shifts to 260 nm for RGO, suggesting that some groups on the GO surface are displaced, and the conjugated structure is restored. The density of π electrons has increased in the reconstructed structure, and with the new arrangement of sp^2 carbons, the structure has a new order [66-67]. RGO–ZnO hybrids band edge absorption is located at 361 nm, almost 9 nm less blue-shifted than the band gap absorption of bulk ZnO at 370 nm. The quantum confinement effect of the smaller feature size of ZnO might explain this issue. Also, a slight blue shift in the absorption peak of RGO-ZnO from 260 to 258 nm is observed comparing pure RGO. Notably, the RGO-ZnO-Fe_2O_4 nanocomposite shows an apparent blue shift and exhibits the absorption edges in 247 nm and 347 nm wavelengths.

The optical absorption coefficient (α) can be calculated using Equation (1),

$$\alpha h\nu = D\left(h\nu - E_g\right)^n \quad (1)$$

where D is constant, $h\nu$ is the incident photon energy, and E_g is the optical band gap and n demonstrates the type of optical transition. In the present case, n=1/2 is considered, which is related to the direct bandgap of prepared material; hence, the plot of $(\alpha h\nu)^2$ versus $h\nu$ is drawn in Fig. 5b. Finally, the bandgap of prepared materials was calculated by extrapolation used on X-axis. The band gaps of GO and RGO are ~3.36 eV and 3.18, respectively. Because some of the oxygen groups are removed in the reduction process, the energy gap can be controlled by managing the correct percentage of oxygen in RGO. The Energy bandgap for pure ZnO is 3.37 eV [68], which then increased to around 3.63 eV with GO. On the other hand, the band gap energy of RGO-ZnO reduced to 3.25 eV due to the increase in the surface charge between ZnO and RGO led to the optical band gap shifting to a higher wavelength [69]. Also, the Eg value for RGO-ZnO-Fe_2O_4 is 2.70 eV, demonstrating that Fe doping has apparently reduced the band gap of RGO-ZnO [70].

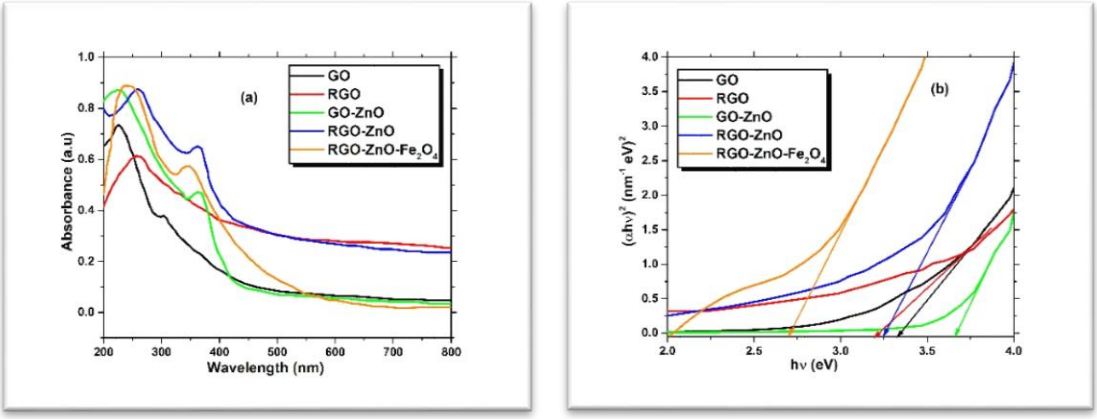

Fig. 5. (a) Absorbance spectra of GO, RGO, RGO-ZnO, and RGO-ZnO-Fe_2O_4 nanocomposite and (b) Bandgap determination according to absorption measurements of GO, RGO, RGO-ZnO, and RGO-ZnO-Fe_2O_4

3.4. Nonlinear Optical Measurement

In photonic devices, linear and nonlinear optical characteristics are of great importance; in this section, the third-order nonlinear optical characteristics of GO, RGO, RGO-ZnO, and RGO-ZnO-Fe_2O_4 samples have been investigated using the Z-scan technique. For this purpose, the second harmonic of a Q-switched Nd: YAG laser (532 nm, 4 ns) was used as the laser source. The sample solutions GO, RGO, RGO-ZnO, and RGO-ZnO-Fe_2O_4 concentrations are 0.2 mg/mL, placed in 1 mm quartz cells. After the light exit, the laser beam was focused by a lens to achieve the maximum intensity at Z=0.

3.5. Nonlinear Optical Properties

As graphene has excellent nonlinear optical properties and optical limiting performance, assessing the NLO properties of metal oxides combined with graphene is important. Graphene has a unique atomic and electronic 2D sheet structure, including sp^2 hybridized carbon atoms. On the other hand, GO is a mainly 2D network with many sp^3 hybridized carbon atoms and some sp^2 domains. The chemical reduction process can develop its concentration. It is reported that highly reduced GO with a more significant percentage of sp^2 carbon domains shows good SA, while partially reduced GO exhibits good RSA characteristics [71]. Due to the existence of prior graphitic nano-islands, which are sp^2-hybridized carbon clusters, the GO has some

properties of graphene. For example, ultrafast carrier dynamics and Pauli blocking cause fast SA in the ultra-broad spectral region. As a result, after being excited by a 532 nm laser, the SA originating from Pauli blocking overcomes the NLO absorption at low pump intensities. According to the small amount of the sp^2 configurations in GO, the contribution of excited state absorption (ESA) originating from small localized sp^2 configurations to the nonlinear absorptive valley should be minor compared to the TPA [72]. The nonlinear absorption (NLA) of GO is mainly originated from two-photon absorption (TPA), resulting from the sp^3 domains; it dominates the NLA at high pump intensities, which is because of the high energy gap of sp^3 bonded carbon (2.7-3.1 eV) [73].

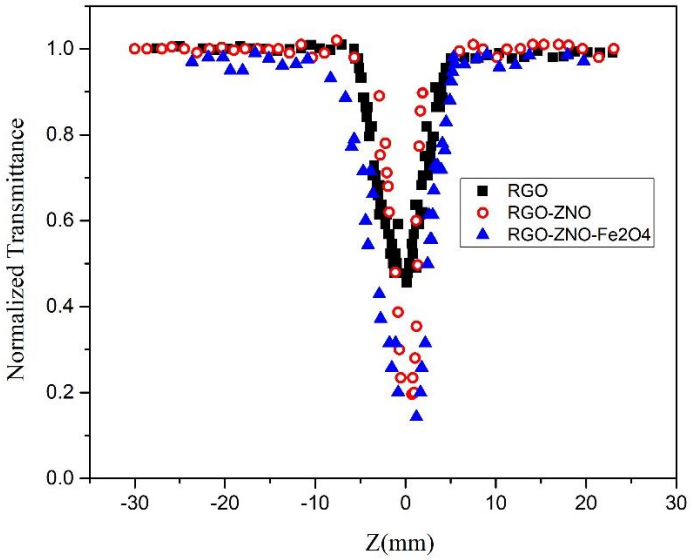

Fig. 6. Open aperture measurements (at 532 nm) of RGO, RGO-ZnO, and RGO-ZnO-Fe_2O_4 at an excitation intensity of 532 nm.

Fig. 6 shows open-aperture Z-scan results of RGO, RGO-ZnO, and RGO-ZnO-Fe_2O_4. It is known that the valley depth of the open aperture Z-scan curve reflects the optical limiting characteristics of the material. If the valley were deeper, its optical limiting performance would be better [73]. As the figure indicates, the normalized transmittance curve of RGO, RGO-ZnO, and RGO-ZnO-Fe_2O_4 samples include valleys, which shows that they exhibit reverse saturable absorption (RSA). The depths of the valleys in the RGO-ZnO and RGO-ZnO-Fe_2O_4 curves are slightly different.

Moreover, the nonlinear absorptive valley of RGO–ZnO and RGO–ZnO-Fe_2O_4 is deeper and broader than RGO, which indicates an increase in NLO properties [73]. Following the reduction, the small localized sp^2 configurations may increase significantly in number but cannot interconnect to form new sp^2 carbon clusters in RGO moiety [72]. The nonlinear absorption coefficient β of RGO, RGO-ZnO, and RGO-ZnO-Fe_2O_4 was investigated. The curves of materials show different trends for nonlinear absorption coefficient β, which should be due to their complicated NLO response mechanisms. After covalent functionalization with Fe, the RGO–ZnO-Fe_2O_4 hybrid exhibits a much higher value of β than RGO. Since, the more significant value of β observed for RGO–ZnO-Fe_2O_4 should have competitively better optical limiting performance [72].

To evaluate the nonlinear optical properties of RGO, RGO-ZnO, and RGO–ZnO-Fe_2O_4 quantitatively, we fit the experimental data with the following equations:

$$T(z) = \sum_{m=0}^{\infty} \frac{(-q_0(z))^m}{(m+1)^{\frac{3}{2}}} \quad (2)$$

$$q_0(z) = \frac{\beta I_0 L_{eff}}{(1+\frac{z^2}{z_0^2})} \quad (3)$$

where T is the open aperture normalized transmittance, $z_0 = \frac{\pi W_0^2}{\lambda}$ is the Rayleigh range, z is the sample position, W_0 is the beam waist at the focal point (Z=0), λ is the laser wavelength, I_0 is the peak intensity, and $L_{eff} = \frac{1-\exp(-\alpha L)}{\alpha}$ is the effective thickness of the sample where α is the linear absorption coefficient of the sample and is calculated from the UV spectrum [73].

Table 1. The value of the nonlinear absorption coefficient obtained from z-scan analysis for GO, RGO, and RGO-ZnO samples.

Sample	I_0 (w/cm)	α (1/cm)	β (cm/w)
RGO	0.05×10^5	0.3	8.3×10^{-4}
RGO-ZnO	0.05×10^5	1.9	8.4×10^{-3}
RGO-ZnO-Fe_2O_4	0.05×10^5	0.6	5.6×10^{-3}

4. Conclusions

We have reported the synthesis, structure, and nonlinear optical properties of GO, RGO, RGO-ZnO, and RGO-ZnO-Fe_2O_4 nanocomposite. The XRD, EDX, FT-IR, and UV–Vis results confirm the successful fabrication of RGO–ZnO-Fe_2O_4. The samples were separately characterized and tested for nonlinear optical properties. The results of open-aperture Z-scan testing on RGO, RGO-ZnO, and RGO–ZnO-Fe_2O_4 indicated the significantly enhancing nonlinear absorption coefficient β values of RGO-ZnO-Fe_2O_4 (5.6×10^{-3} cm/w) compared to RGO. It can be related to combining different NLO mechanisms in RGO–ZnO, including the SA from the sp^2 clusters in the RGO moiety and the RSA originating from the ZnO moiety. Moreover, the Z-scan curve of RGO-ZnO displays a deeper RSA valley. Also, with the increase of the laser light intensity, the nonlinear behavior of the sample changed, and the value of the nonlinear absorption coefficient increased from 1.6×10^{-4} at the intensity of 40 mW to 8.4×10^{-3} at the intensity of 70 mW.

Considering the easy-to-prepare and low-cost RGO–ZnO-Fe_2O_4 nanocomposite and its excellent NLO properties, this research can provide some insight into the design of other novel graphene-based materials for optoelectronic devices such as optical limiting, optical switches, and optical sensors.

References:

[1] T. Kavitha, A.I. Gopalan, K.-P. Lee, S.-Y. Park, Glucose sensing, photocatalytic and antibacterial properties of graphene–ZnO nanoparticle hybrids, Carbon, 50(2012) 2994-3000.

[2] V. Gupta, T.A. Saleh, Syntheses of carbon nanotube-metal oxides composites; adsorption and photo-degradation, Carbon Nanotubes-From Research to Applications, 17(2011) 295-312.

[3] C. Peng, Y. Xiong, Z. Liu, F. Zhang, E. Ou, J. Qian, et al., Bulk functionalization of graphene using diazonium compounds and amide reaction, Applied surface science, 280(2013) 914-9.

[4] H. Miyaji, Y. Kanemoto, A. Hamamoto, K. Shitomi, E. Nishida, A. Kato, et al., Sustained antibacterial coating with graphene oxide ultrathin film combined with cationic surface-active agents in a wet environment, Scientific reports, 12(2022) 1-13.

[5] C. Li, Z. Cheng, J. Gao, Q. Han, M. Ye, J. Zhang, et al., Oxidation degree of graphene reflected by morphology-tailored zno growth, Carbon, 107(2016) 583-92.

[6] T. Giannakopoulou, N. Todorova, A. Erotokritaki, N. Plakantonaki, A. Tsetsekou, C. Trapalis, Electrochemically deposited graphene oxide thin film supercapacitors: Comparing liquid and solid electrolytes, Applied Surface Science, 528(2020) 146801.

[7] R. Jain, A. Sinha, Graphene-zinc oxide nanorods nanocomposite based sensor for voltammetric quantification of tizanidine in solubilized system, Applied Surface Science, 369(2016) 151-8.

[8] H. Wördenweber, S. Karthäuser, A. Grundmann, Z. Wang, S. Aussen, H. Kalisch, et al., Atomically resolved electronic properties in single layer graphene on α-Al2O3 (0001) by chemical vapor deposition, Scientific Reports, 12(2022) 18743.

[9] N. Hameed, L.F. Dumée, F.-M. Allioux, M. Reghat, J.S. Church, M. Naebe, et al., Graphene based room temperature flexible nanocomposites from permanently cross-linked networks, Scientific Reports, 8(2018) 1-8.

[10] Y. Li, G. Zhu, K. Zhou, P. Meng, G. Wang, Evaluation of graphene/crosslinked polyethylene for potential high voltage direct current cable insulation applications, Scientific Reports, 11(2021) 1-8.

[11] K. Sodeinde, S. Olusanya, O. Lawal, M. Sriariyanun, A. Adediran, Enhanced adsorptional-photocatalytic degradation of chloramphenicol by reduced graphene oxide-zinc oxide nanocomposite, Scientific Reports, 12(2022) 1-13.

[12] C.S. Rout, A. Govindaraj, Graphene-based electrochemical supercapacitors.

[13] B.-M. Kim, H.-Y. Kim, S.-W. Hong, W.H. Choi, Y.-W. Ju, J. Shin, Structurally distorted perovskite La0. 8Sr0. 2Mn0. 5Co0. 5O3-δ by graphene nanoplatelet and their composite for supercapacitors with enhanced stability, Scientific reports, 12(2022) 1-8.

[14] K.-H. Choi, H.-J. Nam, J.-A. Jeong, S.-W. Cho, H.-K. Kim, J.-W. Kang, et al., Highly flexible and transparent In Zn Sn O x⁄Ag⁄In Zn Sn O x multilayer electrode for flexible organic light emitting diodes, Applied Physics Letters, 92(2008) 194.

[15] S.H. Raad, Z. Atlasbaf, Solar cell design using

graphene-based hollow nano-pillars, Scientific Reports, 11(2021) 1-8.
[16] J.-K. Chang, Y.-Y. Huang, D.-L. Lin, J.-I. Tau, T.-H. Chen, M.-H. Chen, Solution-processed, semitransparent organic photovoltaics integrated with solution-doped graphene electrodes, Scientific Reports, 10(2020) 1-12.
[17] G. Williams, ACS Nano, 2008, 2, 1487;(e) B. Seger and PV Kamat, J Phys Chem C, 113(2009) 7990.
[18] S. Srikanth, S. Dudala, U. Jayapiriya, J.M. Mohan, S. Raut, S.K. Dubey, et al., Droplet-based lab-on-chip platform integrated with laser ablated graphene heaters to synthesize gold nanoparticles for electrochemical sensing and fuel cell applications, Scientific reports, 11(2021) 1-12.
[19] A.H. Mashhadzadeh, M.G. Ahangari, A. Dadrasi, M. Fathalian, Theoretical studies on the mechanical and electronic properties of 2D and 3D structures of beryllium-oxide graphene and graphene nanobud, Applied Surface Science, 476(2019) 36-48.
[20] Y.-S. Chang, F.-K. Chen, D.-C. Tsai, B.-H. Kuo, F.-S. Shieu, N-doped reduced graphene oxide for room-temperature NO gas sensors, Scientific Reports, 11(2021) 1-12.
[21] T.T. Baby, S. Ramaprabhu, Investigation of thermal and electrical conductivity of graphene based nanofluids, Journal of Applied Physics, 108(2010) 124308.
[22] H. Tao, O.A. Alawi, O.A. Hussein, W. Ahmed, A.H. Abdelrazek, R.Z. Homod, et al., Thermohydraulic analysis of covalent and noncovalent functionalized graphene nanoplatelets in circular tube fitted with turbulators, Scientific Reports, 12(2022) 1-24.
[32] A. Wang, L. Long, W. Zhao, Y. Song, M.G. Humphrey, M.P. Cifuentes, et al., Increased optical nonlinearities of graphene nanohybrids covalently functionalized by axially-coordinated porphyrins, Carbon, 53(2013) 327-38.
[23] P. Khalili, M. Farahmandjou, Study of α-Fe_2O_3 @ ZnO nanoleaves: Morphological and optical study, Materials Engineering Research, 2 (1), (2020)118-124.
[24] H. Zhao, J. Yang, L. Wang, C. Tian, B. Jiang, H. Fu, Fabrication of a palladium nanoparticle/graphene nanosheet hybrid via sacrifice of a copper template and its application in catalytic oxidation of formic acid, Chemical Communications, 47(2011) 2014-6.
[25] B. Ramaraju, C.-H. Li, S. Prakash, C.-C. Chen, Metal–organic framework derived hollow polyhedron metal oxide posited graphene oxide for energy storage applications, Chemical Communications, 52(2016) 946-9.
[26] B. Anasori, M. Beidaghi, Y. Gogotsi, Graphene–transition metal oxide hybrid materials, Mater Today, 17(2014) 253-4.
[27] Z. Wu, Zhou GM Yin L.-C. Ren WC Li F. Cheng H.-M, Nano Energy, 1(2012) 107-31.
[28] X. Fang, J. Liu, J. Wang, H. Zhao, H. Ren, Z. Li, Dual signal amplification strategy of Au nanopaticles/ZnO nanorods hybridized reduced graphene nanosheet and multienzyme functionalized Au@ ZnO composites for ultrasensitive electrochemical detection of tumor biomarker, Biosensors and Bioelectronics, 97(2017) 218-25.
[29] . Benaboud, M. Zaabat, M. Aida, B. Boudine, S. Benzitouni, T. Saidani, Fe_2O_4/ZnO-nanowires synthesis by dip-coating for Orange II-dye photodegradation, Optik, 144 (2017), 397-405.
[30] K. Anand, O. Singh, M.P. Singh, J. Kaur, R.C. Singh, Hydrogen sensor based on graphene/ZnO nanocomposite, Sensors and Actuators B: Chemical, 195(2014) 409-15.
[31] S. Xiong, S. Ye, X. Hu, F. Xie, Electrochemical detection of ultra-trace Cu (II) and interaction mechanism analysis between amine-groups functionalized CoFe2O4/reduced graphene oxide composites and metal ion, Electrochimica Acta, 217(2016) 24-33.
[33] C. Xu, X. Wang, J. Zhu, X. Yang, L. Lu, Deposition of Co 3 O 4 nanoparticles onto exfoliated graphite oxide sheets, Journal of Materials Chemistry, 18(2008) 5625-9.
[34] L.I. Hung, C.K. Tsung, W. Huang, P. Yang, Room- temperature formation of hollow Cu2O nanoparticles, Advanced Materials, 22(2010) 1910-4.
[35] W. Zou, J. Zhu, Y. Sun, X. Wang, Depositing ZnO nanoparticles onto graphene in a polyol system, Materials Chemistry and Physics, 125(2011) 617-20.
[36] X. Wang, H.-F. Wu, Q. Kuang, R.-B. Huang, Z.-X. Xie, L.-S. Zheng, Shape-dependent antibacterial activities of Ag2O polyhedral particles, Langmuir, 26(2010) 2774-8.
[37] X.-L. Wu, L. Wang, C.-L. Chen, A.-W. Xu, X.-K. Wang, Water-dispersible magnetite-graphene-LDH composites for efficient arsenate removal, Journal of Materials Chemistry, 21(2011) 17353-9.
[38] M.S. Ghorashi, H.R. Madaah Hosseini, E. Mohajerani, M. Pedroni, R. Taheri Ghahrizjani, Enhanced TiO2 broadband photocatalytic activity based on very small upconversion nanosystems, The Journal of Physical Chemistry C, 125(2021) 13788-801.
[39] R.T. Ghahrizjani, M.H. Yousefi, Effects of three seeding methods on optimization of temperature, concentration and reaction time on optical properties during growth ZnO nanorods, Superlattices and Microstructures, 112(2017) 10-9.
[40] A. Lakshmanan, P. Surendran, S. S. Priya, K. Balakrishnan, P. Geetha, P. Rameshkumar, T. A.

Hegde, G. Vinitha, K. Kannan, Investigations on structural, optical, dielectric, electronic polarizability, Z-scan and antibacterial properties of Ni/Zn/Fe2O4 nanoparticles fabricated by microwave-assisted combustion method, Journal of Photochemistry and Photobiology A: Chemistry, 402(2020), 112794.
[41] M.-T. Chen, M.-P. Lu, Y.-J. Wu, J. Song, C.-Y. Lee, M.-Y. Lu, et al., Near UV LEDs made with in situ doped pn homojunction ZnO nanowire arrays, Nano letters, 10(2010) 4387-93.
[42] M. McCune, W. Zhang, Y. Deng, High efficiency dye-sensitized solar cells based on three-dimensional multilayered ZnO nanowire arrays with "caterpillar-like" structure, Nano letters, 12(2012) 3656-62.
[43] W. Zhou, J. Zhang, Y. Liu, X. Li, X. Niu, Z. Song, et al., Characterization of anti-adhesive self-assembled monolayer for nanoimprint lithography, Applied Surface Science, 255(2008) 2885-9.
[44] M. Ameri, M. Ghaffarkani, R.T. Ghahrizjani, N. Safari, E. Mohajerani, Phenomenological morphology design of hybrid organic-inorganic perovskite solar cell for high efficiency and less hysteresis, Solar Energy Materials and Solar Cells, 205(2020) 110251.
[45] M. Azadinia, M. Ameri, R.T. Ghahrizjani, M. Fathollahi, Maximizing the performance of single and multijunction MA and lead-free perovskite solar cell, Materials Today Energy, 20(2021) 100647.
[46] R.T. Ghahrizjani, M. Ghafarkani, S. Janghorban, M. Ameri, M. Azadinia, E. Mohajerani, et al., ZnO–SrAl2O4: Eu Nanocomposite-Based Optical Sensors for Luminescence Thermometry, ACS Applied Nano Materials, 4(2021) 9190-9.
[47] A. Amirsalari, A.A. Ziabari, R.T. Ghahrizjani, S.F. Shayesteh, A fundamental study on the effects of nano-silver incorporation on the structure and luminescence properties of color centers in γ′-alumina nanoparticles, Journal of Luminescence, 192(2017) 910-8.
[48] A.R. Sadrolhosseini, E. Ghasami, A. Pirkarimi, S.M. Hamidi, R.T. Ghahrizjani, Highly sensitive surface plasmon resonance sensor for detection of Methylene Blue and Methylene Orange dyes using NiCo-Layered Double Hydroxide, Optics Communications, (2022) 129057.
[49] Y. Hu, J. Zhou, P.H. Yeh, Z. Li, T.Y. Wei, Z.L. Wang, Supersensitive, fast- response nanowire sensors by using Schottky contacts, Wiley Online Library2010.
[50] K. Wang, M. Li, J. Zhang, H. Lu, Polyacrylonitrile coupled graphite oxide film with improved heat dissipation ability, Carbon, 144(2019) 249-58.
[51] W. Gao, The chemistry of graphene oxide, Graphene oxide, Springer2015, pp. 61-95.
[52] U. Hofmann, R. Holst, Über die Säurenatur und die Methylierung von Graphitoxyd, Berichte der deutschen chemischen Gesellschaft (A and B Series), 72(1939) 754-71.
[53] B. Jaleh, A. Jabbari, Evaluation of reduced graphene oxide/ZnO effect on properties of PVDF nanocomposite films, Applied Surface Science, 320(2014) 339-47.
[54] D.C. Marcano, D.V. Kosynkin, Berlin, JM Sinitskii, A, Sun, Z Slesarev, A Alemany, LB Lu and JM Tour Improved synthesis of graphene oxide Acs Nano, 4(2010) 4806.
[55] D.A. Jasim, N. Lozano, K. Kostarelos, Synthesis of few-layered, high-purity graphene oxide sheets from different graphite sources for biology, 2D Materials, 3(2016) 014006.
[56] P. Sengunthar, K. H. Bhavsar, C. Balasubramanian, and U. S. Joshi, Physical properties and enhanced photocatalytic activity of ZnO-rGO nanocomposites, Applied Physics A, 126, (2020) 1-9.
[57] A. S. Merlano, F. Pérez, R. Cabanzo, E. Mejía, L. M. Hoyos, and Á. Salazar, Chemical and morphological analysis of formation of rGO/ZnO composite obtained by microwave-assisted hydrothermal method., Journal of Physics: Conference Series, 1541(2020), 012015.
[58] E. K. Droepenu, B. S. Wee, S. F. Chin, K. Y. Kok, and M. F. Maligan, Zinc oxide nanoparticles synthesis methods and its effect on morphology: A review, Biointerface Res. Appl. Chem, 12, (2022), 4261-4292, 2022.
[59] T. Srinivasulu, K. Saritha, and K. R. Reddy, Synthesis and characterization of Fe-doped ZnO thin films deposited by chemical spray pyrolysis, Modern Electronic Materials, 3, (2017), 76-85, 2017.
[60] W. Wang, S. Guo, D. Zhang, and Z. Yang, One-pot hydrothermal synthesis of reduced graphene oxide/zinc ferrite nanohybrids and its catalytic activity on the thermal decomposition of ammonium perchlorate, Journal of Saudi Chemical Society,.23, (2019), 133-140, 2019.
[61] F. Fajaroh, I. D. Susilowati, and A. Nur, Synthesis of ZnFe2O4 nanoparticles with PEG 6000 and their potential application for adsorbent, in IOP Conference Series: Materials Science and Engineering, 515, (2019), 012049.
[62] M.J. McAllister, J.-L. Li, D.H. Adamson, H.C. Schniepp, A.A. Abdala, J. Liu, et al., Single sheet functionalized graphene by oxidation and thermal expansion of graphite, Chemistry of materials, 19(2007) 4396-404.
[63] Z. Luo, Y. Lu, L.A. Somers, ATC Johnson‖High yield preparation of macroscopic graphen oxide membranes‖, J Am Chem Soc, 131(2009) 898-9.
[64] P. Khanra, T. Kuila, N. Kim, S. Bae, Yu D

sheng, Lee JH, Simultaneous bio-functionalization and reduction of graphene oxide by baker's yeast Chem Eng J, 183(2012) 526-33.
[65] M. Wang, G. Tan, H. Ren, A. Xia, Y. Liu, Direct double Z-scheme Og-C3N4/Zn2SnO4N/ZnO ternary heterojunction photocatalyst with enhanced visible photocatalytic activity, Applied Surface Science, 492(2019) 690-702.
[66] T. Kuila, Saswata Bose, Partha Khanra, Ananta Kumar Mishra, Nam Hoon Kim, and Joong Hee Lee, Biosensors and Bioelectronics, 26(2011) 4637-48.
[67] G. Eda, M. Chhowalla, Chemically derived graphene oxide: towards large- area thin- film electronics and optoelectronics, Advanced materials, 22(2010) 2392-415.
[68] C. Rodwihok, S. Choopun, P. Ruankham, A. Gardchareon, S. Phadungdhitidhada, D. Wongratanaphisan, UV sensing properties of ZnO nanowires/nanorods, Applied Surface Science, 477(2019) 159-65.
[69] R. Kubo, Electronic properties of metallic fine particles. I, Journal of the Physical Society of Japan, 17(1962) 975-86.
[70] S. Nadeem, M. Bukhari, M. Javed, S. Iqbal, M. N. Ahmad, H. Alrbyawi, M. M. Al-Anazy, E. B. Elkaeed, H. Hegazy, M. A. Qayyum, Cation Incorporation and Synergistic Effects on the Characteristics of Sulfur-Doped Manganese Ferrites S@ Mn (Fe_2O_4) Nanoparticles for Boosted Sunlight-Driven Photocatalysis. Molecules, 27 (22), (2022), 7677.
[71] S. Perumbilavil, K. Sridharan, D. Koushik, P. Sankar, V.M. Pillai, R. Philip, Ultrafast and short pulse optical nonlinearity in isolated, sparingly sulfonated water soluble graphene, Carbon, 111(2017) 283-90.
[72] W. Song, C. He, W. Zhang, Y. Gao, Y. Yang, Y. Wu, et al., Synthesis and nonlinear optical properties of reduced graphene oxide hybrid material covalently functionalized with zinc phthalocyanine, Carbon, 77(2014) 1020-30.
[73] P.-l. Li, Y.-h. Wang, M. Shang, L.-f. Wu, X.-X. Yu, Enhanced optical limiting properties of graphene oxide-ZnS nanoparticles composites, Carbon, 159(2020) 1-8.